

Electromagnetic signatures of a strongly coupled anisotropic plasma

Anton Rebhan, Dominik Steineder

*Institut für Theoretische Physik, Technische Universität Wien,
Wiedner Hauptstr. 8–10, 1040 Vienna, Austria*

rebhana@hep.itp.tuwien.ac.at
steineder@hep.itp.tuwien.ac.at

ABSTRACT: In heavy-ion collisions, quark-gluon plasma is likely to be produced with sizable initial pressure anisotropy, which may leave an imprint on electromagnetic observables. In order to model a strongly coupled anisotropic plasma, we use the AdS/CFT correspondence to calculate the current-current correlator of a weakly gauged $U(1)$ subgroup of R symmetry in an $\mathcal{N} = 4$ super-Yang-Mills plasma with a (temporarily) fixed anisotropy. The dual geometry, obtained previously by Janik and Witaszczyk, contains a naked singularity which however permits purely infalling boundary conditions and therefore the usual definition of a retarded correlator. We obtain numerical results for the cases of wave vector parallel and orthogonal to the direction of anisotropy, and we compare with previous isotropic results. In the (unphysical) limit of vanishing frequency (infinite time) we obtain a vanishing DC conductivity for any amount of anisotropy, but the anisotropic AC conductivities smoothly approach the isotropic case in the limit of high frequencies. We also discuss hard photon production from an anisotropic plasma and compare with existing hard-loop resummed calculations.

KEYWORDS: Gauge-gravity correspondence, QCD.

Contents

1. Introduction	1
2. The dual geometry	2
2.1 Review of the Janik-Witaszczyk solution	3
2.2 The appearance of naked singularities	5
3. Current-current correlators and photon production	6
3.1 Basic facts	6
3.2 Introduction of photons and leptons	7
3.3 Tensor structure of anisotropic correlators	8
3.4 Equations of motion and asymptotic solution	8
3.5 Spectral functions at strong coupling	10
4. Numerical results	11
4.1 Wave vector parallel to anisotropy direction	11
4.2 Wave vector perpendicular to anisotropy direction	13
4.3 Conductivities	13
4.4 Anisotropy of traced spectral function for light-like and time-like momenta	14
4.5 Photon and dilepton emission	16
5. Conclusion	18

1. Introduction

Information on the earliest stages of heavy-ion collisions and the production of quark-gluon plasma may be deduced from spectra of photons and dileptons, because real or virtual photons interact only weakly with the surrounding strongly coupled matter [1, 2]. Thermal photon and dilepton production from an isotropic plasma has been studied both in (resummed) perturbation theory [3, 4, 5, 6] and in strongly coupled supersymmetric Yang-Mills plasma by means of gauge/gravity duality [7] (see also [8, 9, 10]).

The angular dependence of photon and dilepton production should carry information on anisotropies present in the plasma prior to isotropization [11, 12, 13, 14, 15, 16, 17], the details of which still remain to be understood. The success of fits of ideal-hydrodynamic simulations [18] suggested time scales of isotropization of $\lesssim 0.7$ fm/c, but later analysis using viscous hydrodynamics found that thermalization may be as late as ~ 2 fm/c, depending significantly on assumptions about the initial conditions [19]. The recent studies

of Ref. [20, 21] suggest that large momentum-space anisotropies may be present for the most part of the time evolution both at weak and strong coupling.

At parametrically weak coupling, a possible framework for carrying out systematic calculations in the nonequilibrium case of an initial momentum space anisotropy is given by the hard-loop effective theory [22] where the backreaction of collective phenomena on the distribution of hard particles is ignored. The latter is either taken as stationary and anisotropic [23, 24, 25, 26, 27, 28, 29], or free streaming with evolving degree of anisotropy [30, 31, 32]. Photon production from Compton-like and annihilation processes in a stationary anisotropic quark-gluon plasma has been studied in [11], confirming expectations of a strong angular dependence. Combined with the time dependence of the momentum space anisotropy, this may even lead to yoctosecond pulses of high-energy photons [33]. Weak-coupling results also exist for energetic dilepton emission from an anisotropic plasma [14], however without inclusion of next-to-leading order effects that become important when dilepton energies are not much higher than temperatures.

In this paper we shall use the AdS/CFT correspondence to study electromagnetic properties of a strongly coupled anisotropic plasma in the approximation of a fixed anisotropy. Like in the weak-coupling situation this should be a reasonable approximation for processes on time-scales smaller than the isotropization time, such as the production of hard photons or dilepton pairs. Following Ref. [34] we study the dual geometry of a stationary anisotropic $N = 4$ supersymmetric Yang-Mills plasma, which contains a naked anisotropic singularity that however still permits purely infalling boundary conditions. We use this setup to generalize the calculation of U(1) current-current spectral functions of Ref. [7] to the anisotropic case. Unlike Ref. [34] we refrain from expansions in the anisotropy parameter, since even the smallest anisotropy changes the character of the fluctuation equations. Indeed, the spectral functions are strongly modified at small frequencies such that the DC conductivity vanishes. The absence of a horizon at any nonzero anisotropy leads to the absence of hydrodynamic behavior, which however just reflects the fact that a stationary anisotropy can only be a good approximation of the nonequilibrium dynamics at sufficiently short time scales. In fact, at large frequencies our results for the spectral function smoothly approach the isotropic limit. This suggests that our setup should permit us to study the effects of temporary anisotropies in a strongly coupled plasma on electromagnetic observables such as hard photon and dilepton spectra.

2. The dual geometry

There has been much progress recently in studying, numerically, the gravity dual of the nonequilibrium dynamics corresponding to analogs of heavy-ion collisions and quark-gluon plasma formation [35, 36, 37, 38, 39, 40, 41, 42], building upon and generalizing the AdS/CFT correspondence of maximally supersymmetric Yang-Mills theory at infinite 't Hooft coupling [43]. Even though all these studies indicate very quick transition to hydrodynamic behavior, estimated to take place at ~ 0.3 fm/c, the results of Ref. [42] show significant anisotropies in the energy-momentum tensor in the subsequent evolution. This is qualitatively in agreement with the analysis of Ref. [20, 21] studying kinetic theory equa-

tions in the presence of momentum space anisotropies at various amounts of specific shear viscosity with the result that both at strong and weak coupling one can expect sizeable pressure anisotropies. Naturally, at weaker coupling (larger viscosity), the anisotropy of the energy-momentum tensor reaches larger degrees and persists for longer times.

Since the AdS/CFT study of electromagnetic spectral functions may be prohibitively difficult in a time-dependent gravity background involving the formation of (time-dependent) horizons, we shall content ourselves with a stationary anisotropic background obtained previously by Janik and Witaszczyk [34].

2.1 Review of the Janik-Witaszczyk solution

According to the AdS/CFT dictionary, the metric of asymptotically anti-de Sitter space in Fefferman-Graham coordinates

$$ds^2 = \frac{\gamma_{\mu\nu}(x^\sigma, z)dx^\mu dx^\nu + dz^2}{z^2}, \quad (2.1)$$

where z is the holographic coordinate, encodes the energy-momentum tensor $\langle T_{\mu\nu}(x^\sigma) \rangle$ of the dual super-Yang-Mills theory through its asymptotic behavior near the boundary at $z = 0$,

$$\gamma_{\mu\nu}(x^\sigma, z) = \eta_{\mu\nu} + z^4 \gamma_{\mu\nu}^{(4)}(x^\sigma) + \mathcal{O}(z^6) \quad (2.2)$$

with

$$\langle T_{\mu\nu}(x^\sigma) \rangle = \frac{N_c^2}{2\pi^2} \gamma_{\mu\nu}^{(4)}(x^\sigma). \quad (2.3)$$

This fixes the boundary condition for the 5-dimensional Einstein equations with a negative cosmological constant

$$R_{MN}(x, z) = -4g_{MN}(x, z) \quad (2.4)$$

and one can solve for the 5-dimensional metric. Requiring nonsingularity of the resulting geometry would allow one to select physical solutions for the profile of the energy-momentum tensor and its time evolution [35, 44, 45].

However we are interested in a stationary anisotropic energy momentum tensor

$$\langle T_{\mu\nu} \rangle = \text{diag}(\epsilon, P_L, P_T, P_T), \quad \langle T^\mu{}_\mu \rangle = 0, \quad (2.5)$$

which we consider as an approximation to the full dynamics at sufficiently short time scales. With these boundary conditions the solution for the metric takes the form

$$ds^2 = \frac{1}{z^2} \left(-a(z)dt^2 + b(z)dx_L^2 + c(z)dx_T^2 + dz^2 \right). \quad (2.6)$$

with

$$\begin{aligned} a(z) &= (1 + A^2 z^4)^{1/2 - \sqrt{36 - 2B^2}/4} (1 - A^2 z^4)^{1/2 + \sqrt{36 - 2B^2}/4} \\ b(z) &= (1 + A^2 z^4)^{1/2 - B/3 + \sqrt{36 - 2B^2}/12} (1 - A^2 z^4)^{1/2 + B/3 - \sqrt{36 - 2B^2}/12} \\ c(z) &= (1 + A^2 z^4)^{1/2 + B/6 + \sqrt{36 - 2B^2}/12} (1 - A^2 z^4)^{1/2 - B/6 - \sqrt{36 - 2B^2}/12}. \end{aligned} \quad (2.7)$$

Table 1: Relation between different anisotropy parameters

B	ξ	P_L/ϵ	P_T/ϵ
-4	-	3	-1
$-\sqrt{6}$	-1	1	0
-1	-0.69675	0.5620	0.2190
-0.1	-0.1160	0.35556	0.3222
0	0	1/3	1/3
0.1	0.1355	0.3111	0.3444
1	4.8102	0.1047	0.4477
$\sqrt{2}$	∞	0	1/2
$\sqrt{12}$	-	-1	1

The parameters A and B are related to the energy density and the pressures according to

$$\begin{aligned}
\epsilon &= \frac{N_c^2}{2\pi^2} \left[\frac{A^2}{2} \sqrt{36 - 2B^2} \right], \\
P_L &= \frac{N_c^2}{2\pi^2} \left[\frac{A^2}{6} \sqrt{36 - 2B^2} - \frac{2A^2B}{3} \right], \\
P_T &= \frac{N_c^2}{2\pi^2} \left[\frac{A^2}{6} \sqrt{36 - 2B^2} + \frac{A^2B}{3} \right].
\end{aligned} \tag{2.8}$$

The anisotropy of the system is parametrized by the dimensionless parameter B . For $B = 0$ we obtain the usual anti-de Sitter/Schwarzschild solution in Fefferman-Graham coordinates. For positive (negative) values of B we obtain an oblate (prolate) anisotropy of the system. P_L and P_T are positive quantities in the range $-\sqrt{6} \leq B \leq \sqrt{2}$, while in the larger interval $-\sqrt{18} < B < \sqrt{18}$ one of the pressure components can be made arbitrarily large and negative. The dimensionful parameter A , which in the isotropic limit equals $\pi^2 T^2/2$, will be set to 1 in the following discussion.

In Table 1 we display the dependence of the pressure components normalized to the energy density as a function of B for a number of values used further below in numerical evaluations. Also given is the connection with the anisotropy parameter ξ introduced in Ref. [46] through one-dimensional deformations of isotropic particle distributions f_{iso} in momentum space,

$$f(\mathbf{p}) = \mathcal{N}(\xi) f_{iso} \left(\sqrt{p^2 + \xi p_L^2} \right), \tag{2.9}$$

with $\mathcal{N}(\xi)$ some normalization factor (e.g., $\mathcal{N} = \sqrt{1 + \xi}$ if the number density is to be kept fixed), and the corresponding energy-momentum tensor in kinetic theory

$$T^{\mu\nu} = N_{\text{eff}} \int \frac{d^3\mathbf{p}}{(2\pi)^3} p^\mu p^\nu f(\mathbf{p}). \tag{2.10}$$

(This of course covers only the range where both P_L and P_T remain positive.)

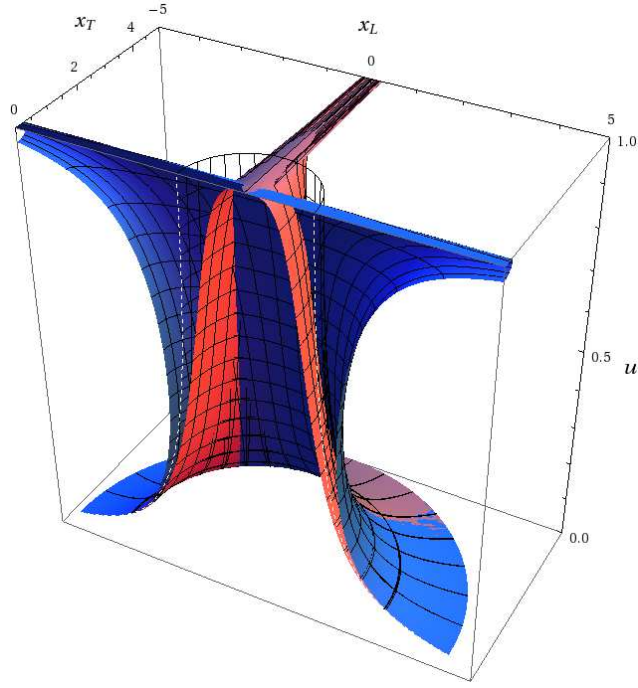


Figure 1: Asymptotically spherical congruences of (holographically) radial light-like geodesics which get deformed into ellipsoids as they approach the singularity at $u = 1$ in units where $A = 1$. The blue (darker) surface corresponds to prolate anisotropy $B = -\sqrt{6}$, the red (lighter) surface to oblate anisotropy $B = \sqrt{2}$, and the transparent mesh to the isotropic case $B = 0$. Here x_T and x_L correspond to the transverse and longitudinal spatial extents of the ellipsoids, which degenerate into an infinite disk or line for oblate or prolate anisotropy, respectively. (Note that x_T is a radial variable.)

Using the analytic expressions for the corresponding ϵ , P_L and P_T of Ref. [31], the relation between ξ and B is given by

$$\frac{\sqrt{36 - 2B^2} + 2B}{\sqrt{36 - 2B^2} - 4B} = \frac{\xi - 1}{2} + \frac{\xi}{(\xi + 1)\xi^{-1/2} \operatorname{atan} \xi^{1/2} - 1}. \quad (2.11)$$

For small anisotropies $\xi = \frac{5}{4}B + O(B^2)$.

2.2 The appearance of naked singularities

For later convenience we write the metric in terms of $u = z^2$:

$$ds^2 = g_{tt}(u)dt^2 + g_{LL}(u)dx_L^2 + g_{TT}(u)d\mathbf{x}_T^2 + g_{uu}(u)du^2, \quad (2.12)$$

$$\begin{aligned} g_{tt}(u) &= -\frac{1}{u}(1 + A^2u^2)^{1/2 - \sqrt{36 - 2B^2}/4}(1 - A^2u^2)^{1/2 + \sqrt{36 - 2B^2}/4} \\ g_{LL}(u) &= \frac{1}{u}(1 + A^2u^2)^{1/2 - B/3 + \sqrt{36 - 2B^2}/12}(1 - A^2u^2)^{1/2 + B/3 - \sqrt{36 - 2B^2}/12} \\ g_{TT}(u) &= \frac{1}{u}(1 + A^2u^2)^{1/2 + B/6 + \sqrt{36 - 2B^2}/12}(1 - A^2u^2)^{1/2 - B/6 - \sqrt{36 - 2B^2}/12} \\ g_{uu}(u) &= \frac{1}{4u^2}. \end{aligned} \quad (2.13)$$

The geometry corresponding to this metric is pathological in the sense that a naked singularity appears whenever B does not vanish. For instance, the induced metric at constant t and $u = 1/A$ is degenerate,

$$g_{LL}g_{TT}^2 \propto (1 - A^2u^2)^{[6 - \sqrt{36 - 2B^2}]/4}. \quad (2.14)$$

Three-dimensional space degenerates at $u = 1/A$ into a two-dimensional sheet when $B > 0$, and into a one-dimensional line when $B < 0$. This is illustrated in Fig. 1 in terms of asymptotically ($u \rightarrow 0$) spherical congruences of holographically radial light-like geodesics. At finite u these are deformed into ellipsoids, which degenerate at $u = 1/A$.

However, in [34] it was noted that it is nevertheless possible to define purely ingoing and outgoing boundary conditions at the naked singularity,¹ which gives the possibility to define retarded correlation functions along the lines of Ref. [47]. In the following we shall do so for current-current correlators of a $U(1)$ current selected from the R -charge currents and assumed to be weakly gauged and thus coupled to electromagnetism.

3. Current-current correlators and photon production

Photons and leptons produced in an early stage after the heavy ion collision interact only very weakly with the medium and can leave the plasma without any rescattering. Therefore the production of photons and dileptons in a strongly coupled plasma is an interesting observable to study the far from equilibrium properties. In isotropic $\mathcal{N} = 4$ SYM plasmas the emission spectra of photons and leptons at strong and weak coupling have been studied in [7]. In the following we shall closely follow this paper and generalize to the above anisotropic background.

3.1 Basic facts

The rate of photons produced per unit time and per unit volume is²

$$d\Gamma_\gamma = \frac{d^3k}{(2\pi)^3} \frac{ie^2}{2|\mathbf{k}|} \eta^{\mu\nu} C_{\mu\nu}^<(K)|_{k^0=|\mathbf{k}|}, \quad (3.1)$$

where

$$C_{\mu\nu}^<(K) = \int d^4X e^{-iK \cdot X} \langle J_\mu^{EM}(0) J_\nu^{EM}(X) \rangle \quad (3.2)$$

is the Wightman function of electromagnetic currents. Any correlator of the conserved current can be expressed in terms of the spectral function, which is defined as

$$\chi_{\mu\nu}(K) = \int d^4X e^{-iK \cdot X} \langle [J_\mu^{EM}(0), J_\nu^{EM}(X)] \rangle. \quad (3.3)$$

¹But the expansion in small B performed in [34] is not really allowed, because the character of the singularities in the equations of motion changes with the anisotropy parameter. We thank Karl Landsteiner for pointing this out to us.

²We use capital letter to denote 4 vectors and lower case letters for the absolute value of 3 vectors. The Minkowski metric is defined as $\eta_{\mu\nu} = \text{diag}(-1, 1, 1, 1)$.

Later we will determine this spectral function by making use of

$$\chi_{\mu\nu}(K) = -2\text{Im}C_{\mu\nu}^{ret}(K). \quad (3.4)$$

The Wightman function is related to the spectral function by

$$C_{\mu\nu}^<(K) = -i\chi_{\mu\nu}(K)\phi(K), \quad (3.5)$$

where ϕ reduces to the Bose-Einstein distribution in thermal equilibrium.

The dilepton production takes place via an intermediate virtual photon and the rate is given by

$$d\Gamma_{l\bar{l}} = \frac{d^4K}{(2\pi)^4} \frac{ie^2 e_l^2 (-K^2 - 4m^2)^{1/2} (-K^2 + 2m^2)}{6\pi |K^2|^{5/2}} \theta(k^0) \theta(-K^2 - 4m^2) \eta^{\mu\nu} C_{\mu\nu}^<(K), \quad (3.6)$$

where e_l is the charge of the lepton. Here the Wightman function must be evaluated for time-like momenta.

3.2 Introduction of photons and leptons

After the brief recapitulation of photon and dilepton production rates in thermal media, we quickly review the possibilities to couple electromagnetism to the $\mathcal{N} = 4$ SYM theory, which consists of $SU(N_c)$ gauge bosons, four Weyl fermions ψ_p and six real scalars $\phi_{pq} = -\phi_{qp}$, all transforming in the adjoint representation of $SU(N_c)$. There is also an anomaly free global $SU(4)$ R -symmetry present, under which the fermions transform in the **4** and the scalars in the **6**. We can take a $U(1)$ subgroup of the $SU(4)$ R -symmetry associated with a $U(1)$ gauge field coupled to the conserved current. By doing so we are able to model the electromagnetic interactions. In principle it is possible to take any linear combination of Cartan subalgebra generators to embed the $U(1)$ in the $SU(4)$ R -symmetry group (for details see [7]). We will choose $t^3 = (1/2, -1/2, 0, 0)$ to be the generator of the $U(1)$ such that two of the Weyl fermions have charge $\pm 1/2$ and two complex scalars have charge $1/2$. The conserved current is

$$J_{\mu}^{EM} = \frac{1}{e} \frac{\delta S_{int}}{\delta A^{\mu}} = \frac{1}{2} \left(\psi_1^{a\dagger} \bar{\sigma}_{\mu} \psi_1^a - \psi_2^{a\dagger} \bar{\sigma}_{\mu} \psi_2^a + \sum_{p=3,4} \phi_{1p}^{a\dagger} (-i\vec{D}_{\mu} + i\overleftarrow{D}_{\mu}) \phi_{1p}^a \right), \quad (3.7)$$

where a is the $SU(N_c)$ group index and the covariant derivative D_{μ} involves the $SU(N_c)$ gauge fields as well as the $U(1)$ electromagnetic vector potential A_{μ} . Because we are only interested in the leading order terms in the electromagnetic coupling e , it is sufficient to treat the electromagnetic interaction as being linear in A_{μ} . Then we can consistently ignore the electromagnetic vector potential in the covariant derivative acting on the scalar. In order to also add weakly coupled leptons l with charge e_l and mass m , the Lagrangian is extended to

$$\mathcal{L} = \mathcal{L}_{SYM} + \mathcal{L}_{int} - \frac{1}{4} F_{\mu\nu}^2 - \bar{l}(\not{D} + m)l \quad \text{with } \mathcal{L}_{int} = e J_{\mu}^3 A^{\mu}, \quad (3.8)$$

where J_{μ}^3 is the t^3 component of the R -current.

In the gauge/gravity setup, only the SYM part will be realized dynamically, but we can calculate current-current correlators to leading order in the electromagnetic coupling and to all orders in the SYM coupling.

3.3 Tensor structure of anisotropic correlators

For an anisotropic medium, the tensor structure of the current-current correlator is more complicated than in the isotropic finite temperature case. Because the electromagnetic current is conserved it must satisfy Ward identities, which implies that any $C_{\mu\nu}(K) \sim P_{\mu\nu}f(K)$ with $P_{\mu\nu} = \eta_{\mu\nu} - K_\mu K_\nu / K^2$.

We begin with the case when the wave vector is pointing in the direction of the anisotropy denoted by $\mathbf{n} = n\mathbf{e}_L$. Then it is sufficient to introduce longitudinal and transverse projectors

$$P_{00}^T = P_{i0}^T = 0, \quad P_{ij}^T = \delta_{ij} - \frac{k_i k_j}{k^2}, \quad P_{\mu\nu}^L = P_{\mu\nu} - P_{\mu\nu}^T. \quad (3.9)$$

For the correlators we then find

$$C_{\mu\nu}(K) = P_{\mu\nu}^T \Pi^T(K) + P_{\mu\nu}^L \Pi^L(K). \quad (3.10)$$

This is exactly the same structure one has in isotropic systems.

If we choose the wave vector to point in a perpendicular direction with respect to the anisotropy $\mathbf{k} = k\mathbf{e}_1$, we need one further tensorial structure,

$$P_{00}^2 = P_{i0}^2 = 0, \quad P_{ij}^2 = \delta_{ij} - \frac{k_i k_j}{k^2} - \frac{n_i n_j}{n^2} \quad (3.11)$$

$$P_{00}^L = P_{i0}^L = 0, \quad P_{ij}^L = \frac{n_i n_j}{n^2} \quad (3.12)$$

$$P_{\mu\nu}^1 = P_{\mu\nu} - P_{\mu\nu}^2 - P_{\mu\nu}^L. \quad (3.13)$$

As a consequence the correlator is then specified by three scalar functions

$$C_{\mu\nu}(K) = P_{\mu\nu}^1 \Pi^1(K) + P_{\mu\nu}^2 \Pi^2(K) + P_{\mu\nu}^L \Pi^L(K). \quad (3.14)$$

With a generic orientation of the wave vector, more structure functions would come into the play. We shall restrict our attention to the two extreme cases of wave vector parallel and orthogonal to the anisotropy direction. It is plausible that the generic case will interpolate smoothly between those two.

3.4 Equations of motion and asymptotic solution

To obtain the retarded correlator we have to solve the equations of motion of a gauge field in the geometry described by (2.12), which are given by

$$\partial_A(\sqrt{-g}g^{AC}g^{BD}F_{CD}) = 0. \quad (3.15)$$

At first we consider the case when the wave vector points in the direction of the anisotropy ($\mathbf{k} = k_L\mathbf{e}_L$). Then the equation of motion for $E_T = \omega A_T$ is

$$E_T'' + \frac{\partial_u(\sqrt{-g}g^{uu}g^{TT})}{\sqrt{-g}g^{uu}g^{TT}}E_T' - \frac{g^{tt}\omega^2 + g^{LL}k_L^2}{g^{uu}}E_T = 0, \quad (3.16)$$

where primes denote derivatives with respect to u and the dependence of u is suppressed everywhere. For the longitudinal electric field $E_L = k_L A_t + \omega A_L$ we find

$$E_L'' + \frac{(g^{tt})^2 \partial_u(\sqrt{-g} g^{uu} g^{LL}) \omega^2 + (g^{LL})^2 \partial_u(\sqrt{-g} g^{uu} g^{tt}) k_L^2}{\sqrt{-g} g^{uu} g^{tt} g^{LL} (g^{tt} \omega^2 + g^{LL} k_L^2)} E_L' - \frac{g^{tt} \omega^2 + g^{LL} k_L^2}{g^{uu}} E_L = 0. \quad (3.17)$$

If the wave vector points in a direction perpendicular to the anisotropy, we obtain three different differential equations. Due to symmetry we are free to choose $\mathbf{k} = k_1 \mathbf{e}_1$ and then find

$$E_2'' + \frac{\partial_u(\sqrt{-g} g^{uu} g^{TT})}{\sqrt{-g} g^{uu} g^{TT}} E_2' - \frac{g^{tt} \omega^2 + g^{TT} k_1^2}{g^{uu}} E_2 = 0 \quad (3.18)$$

$$E_L'' + \frac{\partial_u(\sqrt{-g} g^{uu} g^{LL})}{\sqrt{-g} g^{uu} g^{LL}} E_L' - \frac{g^{tt} \omega^2 + g^{TT} k_1^2}{g^{uu}} E_L = 0 \quad (3.19)$$

for the two modes transverse to the wave vector and

$$E_1'' + \frac{(g^{tt})^2 \partial_u(\sqrt{-g} g^{uu} g^{TT}) \omega^2 + (g^{TT})^2 \partial_u(\sqrt{-g} g^{uu} g^{tt}) k_1^2}{\sqrt{-g} g^{uu} g^{tt} g^{TT} (g^{tt} \omega^2 + g^{TT} k_1^2)} E_1' - \frac{g^{tt} \omega^2 + g^{TT} k_1^2}{g^{uu}} E_1 = 0 \quad (3.20)$$

for the electric field along the direction of the wave vector. These equations are quite lengthy if the explicit form of the metric coefficients is inserted, therefore we will not do so here.

For all of these equations, we can use a Frobenius ansatz near the boundary ($u = 0$) and find the characteristic exponents to be 0 and 1. Close to the naked singularity (which appears exactly where the horizon is in the isotropic case) the differential equations have the following form,

$$\frac{d^2}{du^2} \phi + \frac{C_1}{(1-u)} \frac{d}{du} \phi + \frac{\omega^2 C_2}{(1-u)^\alpha} \phi = 0 \quad (3.21)$$

with $\alpha = (2 + \sqrt{36 - 2B^2})/4 \leq 2$. For isotropic systems $\alpha = 2$ and a Frobenius ansatz is still possible about $u = 1$. In that case we find the characteristic exponents $\pm i\omega/\sqrt{8}$ near the horizon and we can easily define ingoing boundary conditions. For nonvanishing anisotropy $\alpha < 2$ and we can perform a coordinate transformation $x = (1-u)^{(2-\alpha)}$ in order to find appropriate boundary conditions at the naked singularity³. Then the equation of motion is given by

$$\frac{d^2}{dx^2} \phi + \frac{\beta}{x} \frac{d}{dx} \phi + \frac{\gamma^2}{x} \phi = 0 \quad (3.22)$$

where

$$\beta = 1 - \frac{C_1 + 1}{2 - \alpha} \quad \gamma^2 = \frac{C_2 \omega^2}{(2 - \alpha)^2}. \quad (3.23)$$

³Thanks to Karl Landsteiner for clarifying this point.

The solution to this differential equation can be written as

$$\phi(u) \sim (1-u)^{(2-\alpha)(1-\beta)/2} \mathbf{H}_{1-\beta}^{(1,2)}(2\gamma(1-u)^{(2-\alpha)/2}), \quad (3.24)$$

where the Hankel function of the second kind $\mathbf{H}_\nu^{(2)}$ represents ingoing boundary conditions, which we will use for our numerical studies later on.

3.5 Spectral functions at strong coupling

In order to find the on-shell boundary action, we start from the five-dimensional Maxwell action, which is given by

$$S_{5D} = -\frac{1}{4g_B^2} \int \sqrt{-g} g^{AC} g^{BD} F_{AB} F_{CD} \quad (3.25)$$

with $g_B = 16\pi^2 R/N_c^2$ and R the AdS radius. Choosing the gauge $A_u = 0$ we obtain the on-shell boundary term

$$S_B = -\frac{1}{2g_B^2} \int_{u \rightarrow 0} \sqrt{-g} g^{uu} \left(g^{tt} A'_t(K, u) A_t(-K, u) + g^{LL} A'_L(K, u) A_L(-K, u) + g^{TT} \mathbf{A}'_T(K, u) \mathbf{A}_T(-K, u) \right) \quad (3.26)$$

Considering a wave vector pointing into the direction of the anisotropy first, we obtain the relation

$$\omega g^{tt} A'_t(K, u) - k g^{LL} A'_L(K, u) = 0, \quad (3.27)$$

which follows directly from the equations of motion. Inserting this into (3.26) and rewriting the result in terms of electric fields $E_L = \omega A_L + k A_t$ and $\mathbf{E}_T = \omega \mathbf{A}_T$, the boundary term of the action becomes

$$S_B = -\frac{1}{2g_B^2} \int_{u \rightarrow 0} \sqrt{-g} g^{uu} \left(\frac{g^{tt}}{\omega^2 g^{tt}/g^{LL} + k^2} E'_L(K, u) E_L(-K, u) + \frac{g^{TT}}{\omega^2} \mathbf{E}'_T(K, u) \mathbf{E}_T(-K, u) \right). \quad (3.28)$$

The transverse correlator is defined as

$$C_{TT}(K) = \frac{\delta^2 S_B}{\delta A_T(K) \delta A_T(-K)} = \frac{\omega^2 \delta^2 S_B}{\delta E_T(K) \delta E_T(-K)}. \quad (3.29)$$

Applying the Lorentzian AdS/CFT prescription [47] and inserting the explicit form of the metric coefficients we find

$$C_{TT}(K) = \Pi_{TT}(K) = -\frac{2}{g_B^2} \lim_{u \rightarrow 0} \frac{E'_T(K, u)}{E_T(K, u)}. \quad (3.30)$$

After a similar computation for the longitudinal correlator we find

$$\Pi_L(K) = -\frac{2}{g_B^2} \lim_{u \rightarrow 0} \frac{E'_L(K, u)}{E_L(K, u)}. \quad (3.31)$$

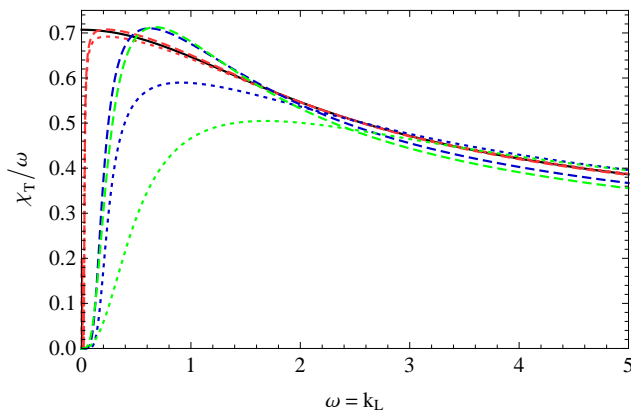


Figure 2: Transverse contribution to spectral density for light-like momenta with values for the anisotropy parameter $B = 0$ (black), $B = 0.1$ (red, dashed), $B = -0.1$ (red, dotted), $B = 1$ (blue, dashed), $B = -1$ (blue, dotted), $B = \sqrt{2}$ (green, dashed) and $B = -\sqrt{6}$ (green, dotted). The dimensionful parameter A , which equals $\pi^2 T^2/2$ in the isotropic case $B = 0$, has been set to unity.

When the wave vector is in the 1-direction we obtain three scalar functions which are given by

$$\Pi_a(K) = -\frac{2}{g_B^2} \lim_{u \rightarrow 0} \frac{E'_a(K, u)}{E_a(K, u)}, \quad (3.32)$$

with $a = 1, 2, L$. Notice that the equations of motion for E_L differ for wave vector perpendicular and parallel to the direction of anisotropy, cf. (3.17) and (3.19).

4. Numerical results

4.1 Wave vector parallel to anisotropy direction

First we discuss the form of the spectral function for a wave vector parallel to the anisotropy direction. When we consider light-like momenta only the transverse contribution to the spectral density is nonvanishing. The results for different anisotropy parameters are shown in Fig. 2. The black line corresponds to the isotropic case and coincides with the spectral density presented in [7] after the correct normalization is chosen. For nonvanishing anisotropy we notice a qualitative difference for small frequencies, namely all spectral functions tend to zero faster than ω , which is in stark contrast to the isotropic situation. However for small values of B the curve quickly rises and then settles close to the isotropic one. For increasing anisotropy the spectral densities deviate more strongly from the isotropic result, in particular at small frequencies.

Since small frequencies correspond to long time scales, the approximation of a stationary anisotropy is bound to break down in this limit. On the other hand, at larger frequencies our analysis should be able to map the nonequilibrium situation in the form of a snapshot, so it is reassuring that there the effects of the anisotropy connect smoothly with the isotropic limit. Given that the appearance of the naked singularity is not a small

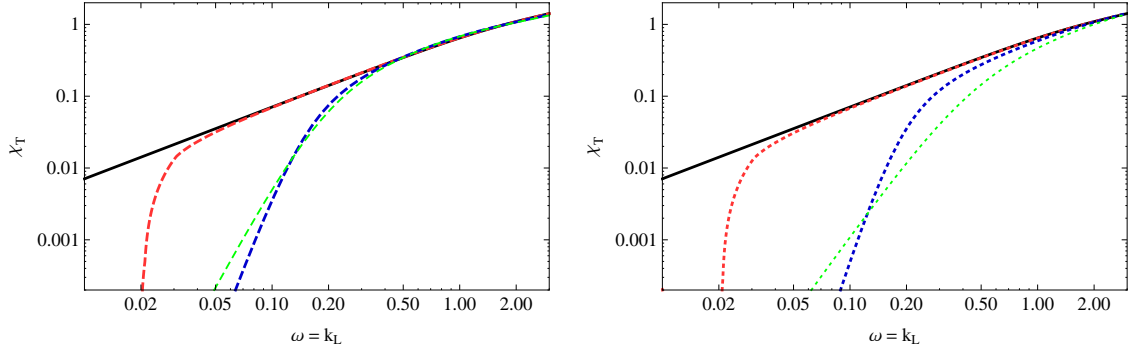


Figure 3: Double logarithmic plot to estimate the deviation from the linear behavior of the spectral function with respect to ω . In the left panel we consider positive anisotropies and in the right panel negative ones. Color coding as in Fig. 2

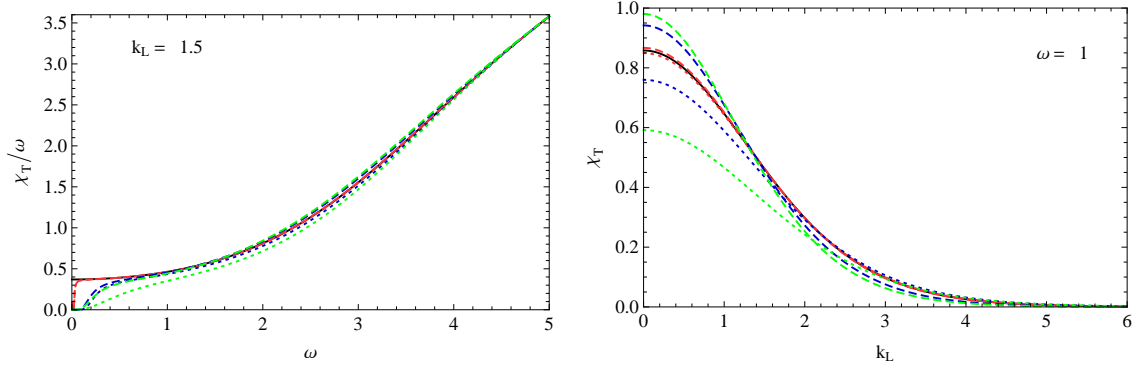


Figure 4: Transverse spectral function for k_L fixed (left) and ω fixed (right). Color coding as in Fig. 2

modification as it changes the character of the differential equations, this is not completely obvious a priori.

Since the low frequency limit seems to be unphysical, the question arises down to what value of ω we might trust this calculation. It makes sense to assume that the lower bound of the frequency will depend on the anisotropy of the system. For larger anisotropies our assumption of a time invariant background may break down earlier. A possible hint to estimate the range of validity of the calculation presented here can come from considering the deviation from $\chi \propto \omega$ as is done in Fig. 3. We see that even for the most extreme anisotropy parameters this suggests our calculation to be valid down to $\omega \sim 1$ (in units where $A = 1$).

In Fig. 4 the form of the transverse part of the spectral function is shown for k_L fixed and ω fixed, respectively. In the left panel the difference in the small frequency behavior between isotropic and anisotropic results is again obvious.

As already mentioned the longitudinal part of spectral density vanishes for light-like momenta. This is still the case if we turn on the anisotropy. In Fig. 5 we see that the

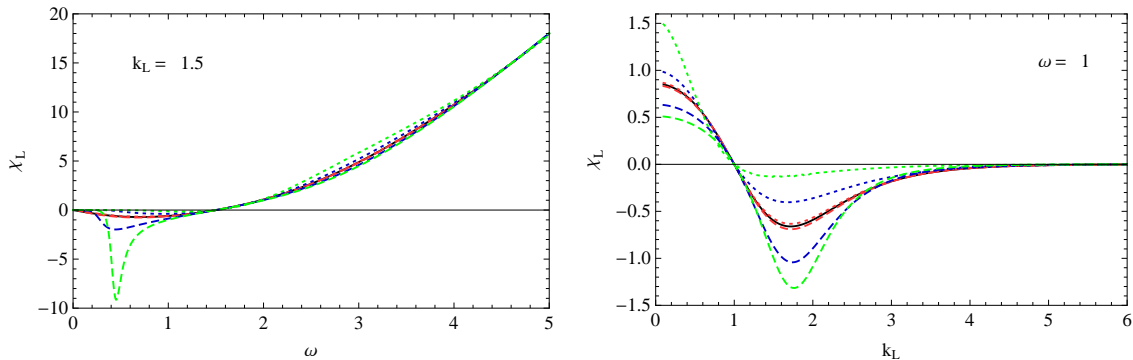


Figure 5: Longitudinal spectral function for k_L fixed (left) and ω fixed (right). Color coding as in Fig. 2

spectral function is negative for space-like momenta, vanishes for light-like momenta and becomes positive for time-like momenta.⁴

4.2 Wave vector perpendicular to anisotropy direction

Next we consider a wave vector pointing in the 1-direction. Then there is a mode which is both, perpendicular to the wave vector and the anisotropy direction. This mode can be compared to the transverse mode before and we see that the behavior for small frequencies and wave vectors is quite similar. The spectral function is larger for oblate anisotropy and smaller for prolate. However, while this is still true for larger frequencies and momenta in the present case (see Fig. 6 and 7), the opposite was true for χ_T , where the behavior changed at some intermediate frequency or momentum.

For $\mathbf{k} = k_1 \mathbf{e}_1$ there is another mode which is transverse with respect to the wave vector. The results for this mode, which is pointing along the anisotropy direction are shown in Fig. 8 and 9. Compared to the previous modes that were transverse with respect to the wave vector, the dependence on B changed. Here the spectral density is larger for prolate anisotropy and smaller in the oblate case.

Finally we can consider the mode longitudinal to the wave vector. The behavior is shown in Fig. 10. The spectral density for light-like momenta vanishes, as it should.

4.3 Conductivities

The fact that for any nonzero anisotropy parameter B all spectral functions tend to zero stronger than linearly in the limit $\omega \rightarrow 0$ means that both the diffusion constant and the DC conductivity vanish according to Kubo’s formulae. This absence of hydrodynamic

⁴It turned out to be hard to solve the differential equations in the longitudinal cases numerically. While the default setting of Mathematica’s NDSolve produces error messages at some data points, but matches with most of the other methods whenever no error occurs, the so called “StiffnessSwitching” method produces no errors at all but sometimes produces very different results from the other methods. We circumvented the difficulties by using the default method and computing many data points, such that we can safely neglect all the data points producing an error message. The final plots do not change when the number of data points is further increased.

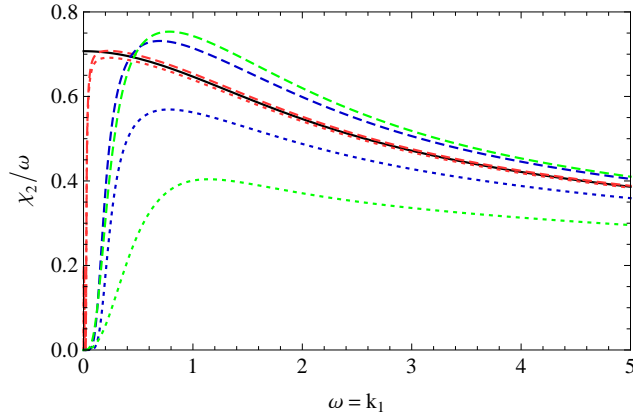


Figure 6: Part of spectral density perpendicular to k_1 and to the anisotropy direction for light-like momenta. Color coding as in Fig. 2

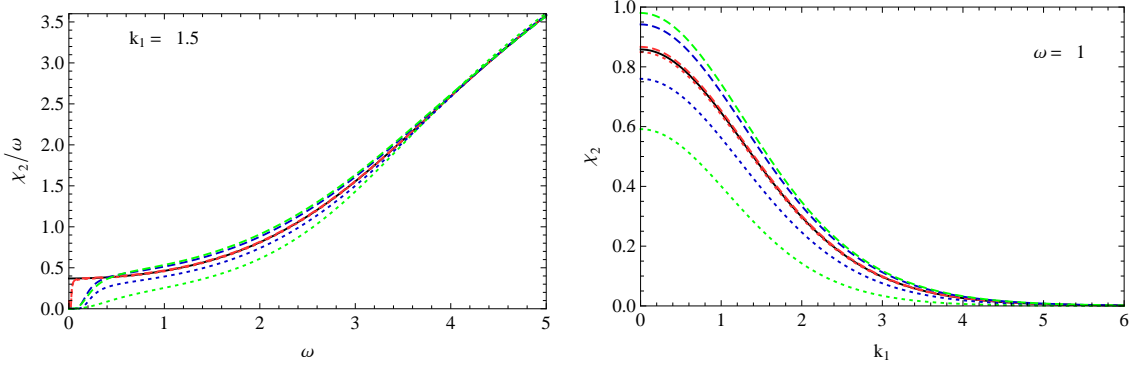


Figure 7: Contribution to spectral function which is perpendicular to the wave vector and the anisotropy direction for k_1 fixed (left) and ω fixed (right). Color coding as in Fig. 2

behavior is clearly related to the absence of a horizon, which for $B \neq 0$ gets replaced by a naked singularity.

In Fig. 11 we display the results for the AC conductivities, juxtaposed for the cases of prolate ($B < 0$) and oblate ($B > 0$) anisotropies. In each case one can define longitudinal and transverse conductivities with respect to the direction of anisotropy. For prolate anisotropies transverse conductivities are found to be reduced compared to the isotropic case, whereas for oblate anisotropies this is true for longitudinal conductivities. However, in the limit of vanishing frequency, all conductivities go to zero. The frequency range in which this happens increases as the amount of anisotropy is increased, up to the point where one of the pressure components goes to zero. Curiously, when increasing the anisotropy parameter such that also negative pressures are produced, this trend is eventually reversed.

4.4 Anisotropy of traced spectral function for light-like and time-like momenta

The production of real photons is proportional to the trace of the spectral functions for

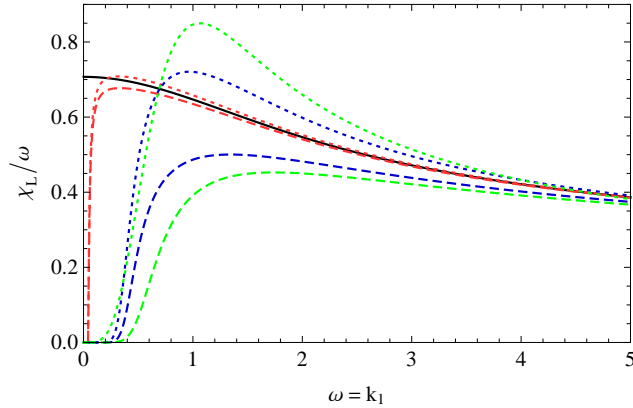


Figure 8: Spectral function along the anisotropy direction for light-like momenta. Color coding as in Fig. 2

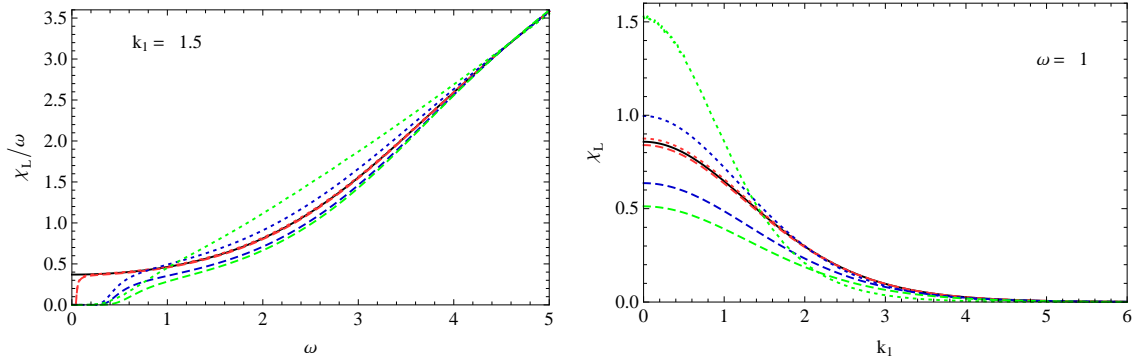


Figure 9: Contribution to spectral function parallel to the anisotropy direction for k_1 fixed (left) and ω fixed (right). Color coding as in Fig. 2

light-like momenta. When the wave vector is parallel to the anisotropy direction, we have

$$\chi^\mu{}_\mu(\mathbf{k} = k_L \mathbf{e}_L, K^2 = 0) = 2\chi_T(k_L), \quad (4.1)$$

whereas for transverse wave vector,

$$\chi^\mu{}_\mu(\mathbf{k} = k_1 \mathbf{e}_1, K^2 = 0) = \chi_2(k_1) + \chi_L(k_1). \quad (4.2)$$

In Fig. 12 the results for the wave vector pointing parallel and perpendicular to the anisotropy direction are juxtaposed, and in Fig. 13 the ratio between the latter and the former is shown as a function of frequency and anisotropy parameter B .

For frequencies $\omega \lesssim 1$ (in units where $A = 1$) this ratio shows a rather dramatic dependence on the anisotropy parameter. However, as we have discussed above, we consider this regime to be unphysical since the assumption of stationarity of the anisotropic plasma ceases to make sense. For larger frequencies we indeed find a smoother dependence on the anisotropy parameter. For positive B (oblate anisotropy) the spectral function with wave vector pointing in the direction of anisotropy is reduced, for negative B the situation is

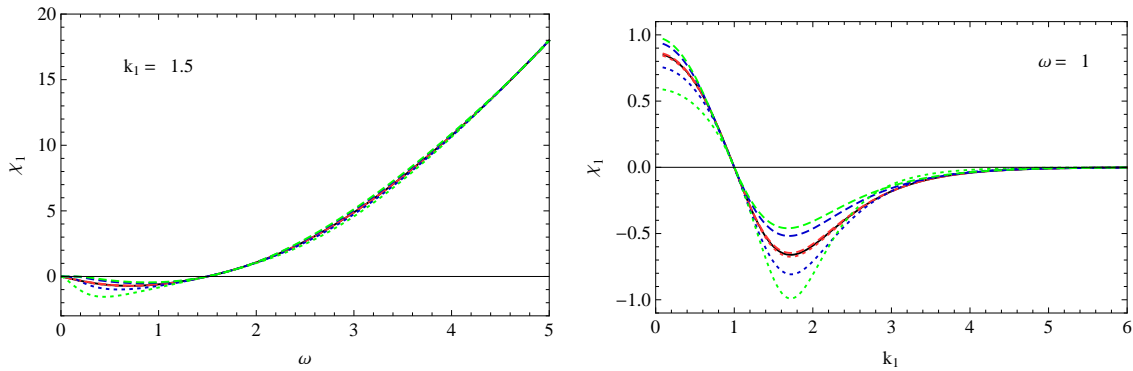


Figure 10: Spectral function longitudinal to the wave vector for k_1 fixed (left) and ω fixed (right). Color coding as in Fig. 2

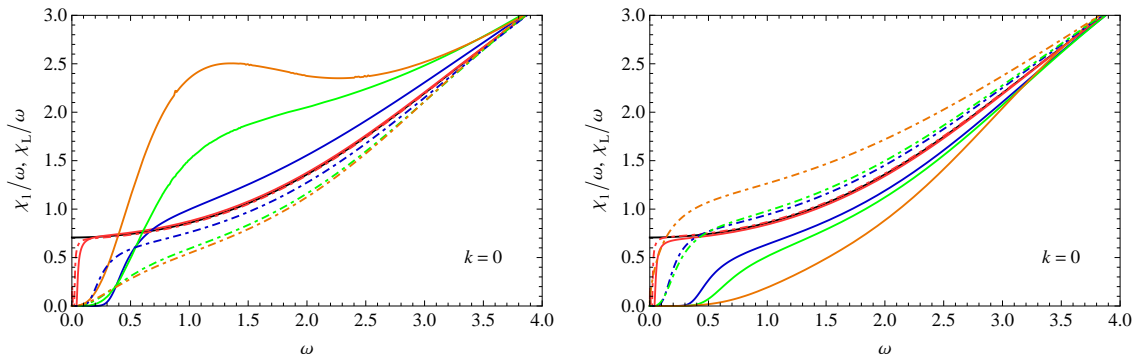


Figure 11: Anisotropic AC conductivities: prolate vs. oblate anisotropies for various values of B . Full lines correspond to longitudinal conductivity, dashed lines to transverse conductivity. Color coding of B as in Fig. 2, with the addition of orange lines for $B = \mp 3$, values for which negative pressures arise.

reversed. As we shall discuss below, this is in line with the behavior of particle distributions for corresponding momentum anisotropies, but the latter typically have exponential suppression at high momentum.

In Fig. 14 we display the behavior of $\chi^\mu{}_\mu$ for time-like momenta, which is relevant for dilepton production, as a function of k_L and k_1 for the two cases of longitudinal and transverse momentum at a fixed value of $K^2 = 1$.

4.5 Photon and dilepton emission

In order to obtain the photon and dilepton production rates, we must insert the results for the spectral function into (3.1) and (3.6), respectively. For the final result we would also need to know the distribution function ϕ , which in the out-of-equilibrium situation is no longer fixed to the Bose-Einstein function. Absent the fluctuation-dissipation theorem, we should therefore calculate the Wightman function within the gauge/gravity duality framework directly. Attempts to incorporate the full formalism of nonequilibrium physics

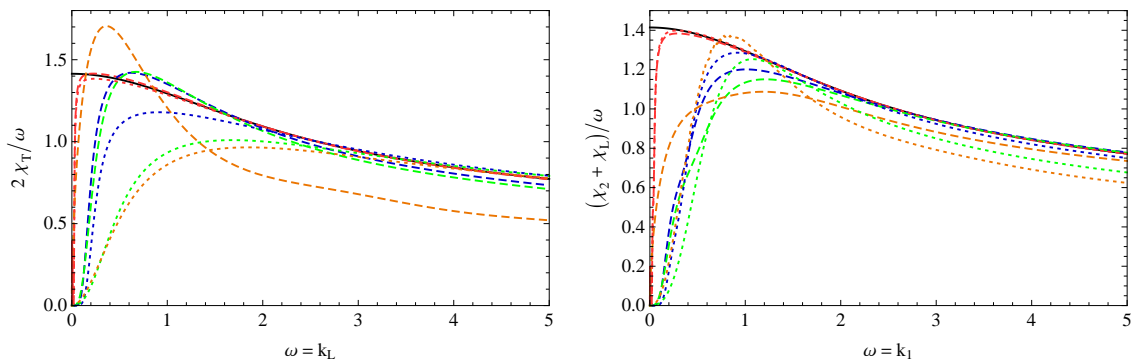


Figure 12: χ^μ_μ/ω for light-like momenta with wave vector parallel to the anisotropy direction (left panel) and transverse to it (right panel). Color coding of B as in Fig. 11

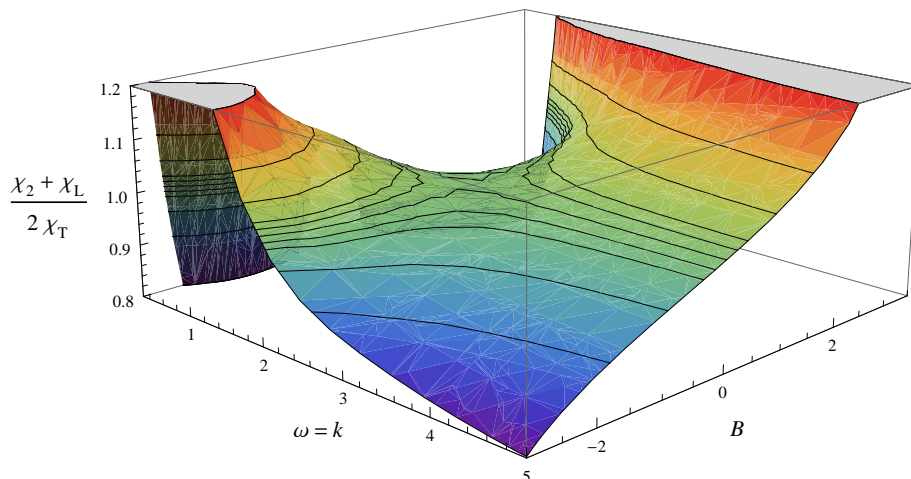


Figure 13: Ratio of χ^μ_μ for light-like momenta with transverse wave vector over this quantity with parallel wave vector (w.r.t. the direction of anisotropy) as a function of both frequency and anisotropy parameter B .

in the AdS/CFT correspondence were undertaken in [48, 49], but we have not been able to apply these concepts to our case.

We shall instead make an estimate of photon and dilepton emission rates by assuming that the distribution function ϕ is given by the form (2.9) with a parameter ξ that at weak coupling gives the same energy momentum tensor as in the boundary field theory of our gravity duality (see eq. (2.11)). Since the distribution function (2.9) depends exponentially on the angle, the overall normalization constant $\mathcal{N}(\xi)$ does not play an important role. Because the energy density at strong coupling, eq. (2.8), depends rather weakly on the anisotropy parameter B , we have fixed $\mathcal{N}(\xi)$ such that the energy density at weak coupling remains constant as ξ and B are varied.

In Fig. 15 we display the resulting photon production rates in longitudinal and transverse directions for small and medium anisotropies. The left panel shows the situation for

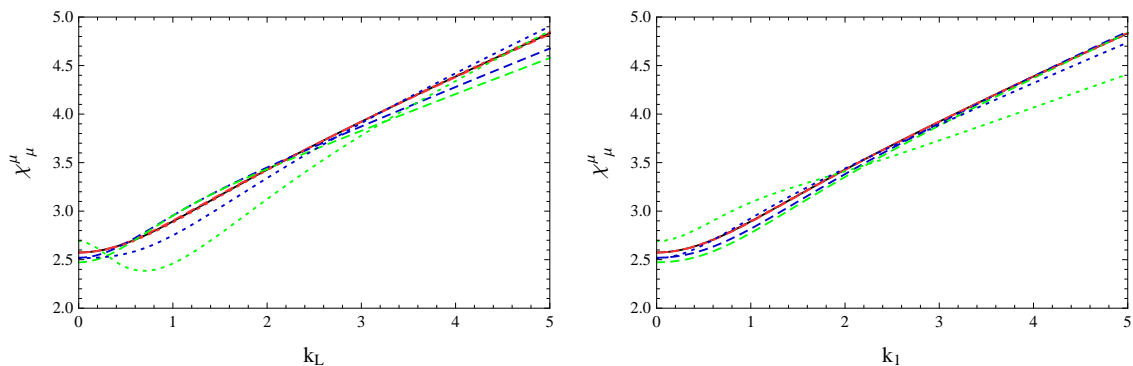


Figure 14: $\chi^\mu{}_\mu$ for time-like momenta with invariant mass $K^2 = 1$ as a function of k_L and k_1 , respectively. Color coding as in Fig. 2

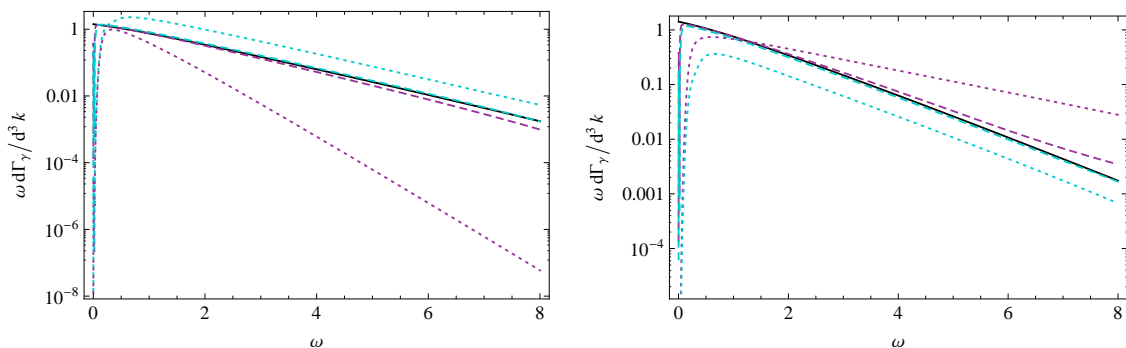


Figure 15: Photon production rate in forward (purple) and transverse (cyan) direction for $B = \pm 0.1$ (dashed) and $B = \pm 1$ (dotted), where positive signs (oblate cases) correspond to the plot on the left and negative signs (prolate cases) are shown in the right panel. As a reference the isotropic rate is given in black.

oblate anisotropies ($B = 0.1$ and 1), the right panel for prolate anisotropies ($B = -0.1$ and -1). This agrees qualitatively with the corresponding result for oblate anisotropies in the weak coupling (hard-loop resummed) calculation of Ref. [11].⁵ Similar results are obtained for production rates of dileptons. The angular dependence in both cases is dominated by the function ϕ when it is chosen in accordance to the situation at weak coupling.

5. Conclusion

In this work we have generalized the AdS/CFT calculation of electromagnetic observables in strongly coupled $\mathcal{N} = 4$ super-Yang-Mills theory in thermal equilibrium of Ref. [7]

⁵Our estimated result for real photon production is in fact more strongly suppressed in the forward direction than the result of Ref. [11]. It shares this behavior with the soft part of the full result of Ref. [11], which in the forward direction is dominated by hard contributions. The final result of Ref. [11] actually depends on the choice of a separation parameter of hard and soft scales which was fixed by a minimization procedure in the isotropic case. Fixing it instead anew for each value of ξ would further reduce the hard-loop result in the forward direction.

to the case of a stationary anisotropic plasma using the singular geometry of Janik and Witaszczyk [34]. In contrast to the latter work, we have refrained from an expansion in the anisotropy parameter since any nonzero anisotropy changes qualitatively the character of the fluctuation equations. In the limit of small frequencies, we have found that for any amount of anisotropy the hydrodynamic behavior of spectral functions is lost, whereas at higher frequencies deviations from the isotropic case are smooth. This reflects the fact that a stationary anisotropic geometry can only be viewed as a reasonable approximation to the early stage of plasma formation and thermalization when the involved time scales are sufficiently short.

We have worked out the independent spectral functions of the electromagnetic current-current correlation tensor (defined by a weakly gauged U(1) subgroup of the R symmetry) and their dependence on anisotropy parameter and wave vector. Absent a recipe for directly calculating Wightman functions, we have estimated photon production rates by adopting deformed thermal distributions that have previously been employed in weak coupling calculations. Doing so, our results turned out to be qualitatively similar to the weak coupling results of [11] in that an oblate anisotropy leads to a strong suppression in the forward direction. It would of course be very desirable to have a direct calculation of Wightman functions in our nonequilibrium geometry which so far has been achieved only in few cases [48, 49, 50].

Recently a different gravity dual for anisotropic plasmas has been proposed in Refs. [51, 52] which is based on geometries dual to Lifshitz-like fixed points constructed in Ref. [53]. This approach involves additional bulk fields and thereby achieves completely regular geometries. It would be very interesting to compare spectral functions of current-current correlators obtained in this approach with our results. We would expect that the two approaches should agree in the regime of high frequencies but deviate in the infrared. However, in the latter regime neither of the two approaches will provide a consistent model of a strongly coupled anisotropic plasma, since the time dependence of the anisotropy can no longer be ignored.

Acknowledgments

We thank Rolf Baier, Karl Landsteiner, Björn Schenke, and Mike Strickland for helpful discussions. This work was supported by the Austrian Science Foundation FWF, project no. P22114, and ÖAD, project no. ES 12/2009.

References

- [1] F. Arleo, P. Aurenche, F. W. Bopp, I. Dadić, G. David, *et. al.*, *Hard probes in heavy-ion collisions at the LHC: Photon physics in heavy ion collisions at the LHC*, [hep-ph/0311131](#). Writeup of the working group Photon Physics for the CERN Yellow Report on Hard Probes in Heavy Ion Collisions at the LHC.
- [2] P. Stankus, *Direct photon production in relativistic heavy-ion collisions*, *Ann.Rev.Nucl.Part.Sci.* **55** (2005) 517–554.
- [3] P. Aurenche, F. Gelis, R. Kobes, and H. Zaraket, *Bremsstrahlung and photon production in thermal QCD*, *Phys.Rev.* **D58** (1998) 085003, [[hep-ph/9804224](#)].

- [4] P. B. Arnold, G. D. Moore, and L. G. Yaffe, *Photon emission from quark gluon plasma: Complete leading order results*, *JHEP* **0112** (2001) 009, [[hep-ph/0111107](#)].
- [5] P. B. Arnold, G. D. Moore, and L. G. Yaffe, *Photon and gluon emission in relativistic plasmas*, *JHEP* **0206** (2002) 030, [[hep-ph/0204343](#)].
- [6] J.-P. Blaizot and F. Gelis, *Photon and dilepton production in the quark-gluon plasma: Perturbation theory vs lattice QCD*, *Eur.Phys.J.* **C43** (2005) 375–380, [[hep-ph/0504144](#)].
- [7] S. Caron-Huot, P. Kovtun, G. D. Moore, and L. G. Starinets, Andrei and, *Photon and dilepton production in supersymmetric Yang-Mills plasma*, *JHEP* **0612** (2006) 015, [[hep-th/0607237](#)].
- [8] A. Parnachev and D. A. Sahakyan, *Photoemission with Chemical Potential from QCD Gravity Dual*, *Nucl.Phys.* **B768** (2007) 177–192, [[hep-th/0610247](#)].
- [9] D. Mateos and L. Patino, *Bright branes for strongly coupled plasmas*, *JHEP* **0711** (2007) 025, [[arXiv:0709.2168](#)].
- [10] A. Nata Atmaja and K. Schalm, *Photon and Dilepton Production in Soft Wall AdS/QCD*, *JHEP* **1008** (2010) 124, [[arXiv:0802.1460](#)].
- [11] B. Schenke and M. Strickland, *Photon production from an anisotropic quark-gluon plasma*, *Phys.Rev.* **D76** (2007) 025023, [[hep-ph/0611332](#)].
- [12] A. Ipp, A. Di Piazza, J. Evers, and C. H. Keitel, *Photon polarization as a probe for quark-gluon plasma dynamics*, *Phys.Lett.* **B666** (2008) 315–319, [[arXiv:0710.5700](#)].
- [13] M. Martinez and M. Strickland, *Measuring QGP thermalization time with dileptons*, *Phys.Rev.Lett.* **100** (2008) 102301, [[arXiv:0709.3576](#)].
- [14] M. Martinez and M. Strickland, *Pre-equilibrium dilepton production from an anisotropic quark-gluon plasma*, *Phys.Rev.* **C78** (2008) 034917, [[arXiv:0805.4552](#)].
- [15] M. Martinez and M. Strickland, *Suppression of forward dilepton production from an anisotropic quark-gluon plasma*, *Eur.Phys.J.* **C61** (2009) 905–913, [[arXiv:0808.3969](#)].
- [16] L. Bhattacharya and P. Roy, *Measuring isotropization time of Quark-Gluon-Plasma from direct photon at RHIC*, *Phys.Rev.* **C79** (2009) 054910, [[arXiv:0812.1478](#)].
- [17] L. Bhattacharya and P. Roy, *Rapidity distribution of photons from an anisotropic Quark-Gluon-Plasma*, *Phys.Rev.* **C81** (2010) 054904, [[arXiv:0907.3607](#)].
- [18] P. Huovinen, P. Kolb, U. W. Heinz, P. Ruuskanen, and S. Voloshin, *Radial and elliptic flow at RHIC: Further predictions*, *Phys.Lett.* **B503** (2001) 58–64, [[hep-ph/0101136](#)].
- [19] M. Luzum and P. Romatschke, *Conformal Relativistic Viscous Hydrodynamics: Applications to RHIC results at $s(NN)^{1/2} = 200$ -GeV*, *Phys.Rev.* **C78** (2008) 034915, [[arXiv:0804.4015](#)].
- [20] M. Martinez and M. Strickland, *Dissipative Dynamics of Highly Anisotropic Systems*, *Nucl.Phys.* **A848** (2010) 183–197, [[arXiv:1007.0889](#)].
- [21] M. Martinez and M. Strickland, *Non-boost-invariant anisotropic dynamics*, *Nucl.Phys.* **A856** (2011) 68–87, [[arXiv:1011.3056](#)].
- [22] S. Mrowczynski, A. Rebhan, and M. Strickland, *Hard loop effective action for anisotropic plasmas*, *Phys.Rev.* **D70** (2004) 025004, [[hep-ph/0403256](#)].

- [23] A. Rebhan, P. Romatschke, and M. Strickland, *Hard-loop dynamics of non-Abelian plasma instabilities*, *Phys.Rev.Lett.* **94** (2005) 102303, [[hep-ph/0412016](#)].
- [24] P. B. Arnold, G. D. Moore, and L. G. Yaffe, *The Fate of non-Abelian plasma instabilities in 3+1 dimensions*, *Phys.Rev.* **D72** (2005) 054003, [[hep-ph/0505212](#)].
- [25] A. Rebhan, P. Romatschke, and M. Strickland, *Dynamics of quark-gluon-plasma instabilities in discretized hard-loop approximation*, *JHEP* **0509** (2005) 041, [[hep-ph/0505261](#)].
- [26] P. B. Arnold and G. D. Moore, *QCD plasma instabilities: The NonAbelian cascade*, *Phys.Rev.* **D73** (2006) 025006, [[hep-ph/0509206](#)].
- [27] D. Bödeker and K. Rummukainen, *Non-abelian plasma instabilities for strong anisotropy*, *JHEP* **0707** (2007) 022, [[arXiv:0705.0180](#)].
- [28] P. B. Arnold and G. D. Moore, *Non-Abelian plasma instabilities for extreme anisotropy*, *Phys.Rev.* **D76** (2007) 045009, [[arXiv:0706.0490](#)].
- [29] A. Ipp, A. Rebhan, and M. Strickland, *Non-Abelian plasma instabilities: SU(3) vs. SU(2)*, [arXiv:1012.0298](#).
- [30] P. Romatschke and A. Rebhan, *Plasma Instabilities in an Anisotropically Expanding Geometry*, *Phys.Rev.Lett.* **97** (2006) 252301, [[hep-ph/0605064](#)].
- [31] A. Rebhan, M. Strickland, and M. Attems, *Instabilities of an anisotropically expanding non-Abelian plasma: 1D+3V discretized hard-loop simulations*, *Phys.Rev.* **D78** (2008) 045023, [[arXiv:0802.1714](#)].
- [32] A. Rebhan and D. Steineder, *Collective modes and instabilities in anisotropically expanding ultrarelativistic plasmas*, *Phys.Rev.* **D81** (2010) 085044, [[arXiv:0912.5383](#)].
- [33] A. Ipp, C. H. Keitel, and J. Evers, *Yoctosecond photon pulses from quark-gluon plasmas*, *Phys.Rev.Lett.* **103** (2009) 152301, [[arXiv:0904.4503](#)].
- [34] R. A. Janik and P. Witaszczyk, *Towards the description of anisotropic plasma at strong coupling*, *JHEP* **0809** (2008) 026, [[arXiv:0806.2141](#)].
- [35] R. A. Janik and R. B. Peschanski, *Asymptotic perfect fluid dynamics as a consequence of AdS/CFT*, *Phys.Rev.* **D73** (2006) 045013, [[hep-th/0512162](#)].
- [36] Y. V. Kovchegov and A. Taliotis, *Early Time Dynamics in Heavy Ion Collisions from AdS/CFT Correspondence*, *Phys.Rev.* **C76** (2007) 014905, [[arXiv:0705.1234](#)].
- [37] D. Grumiller and P. Romatschke, *On the collision of two shock waves in AdS(5)*, *JHEP* **0808** (2008) 027, [[arXiv:0803.3226](#)].
- [38] P. M. Chesler and L. G. Yaffe, *Horizon formation and far-from-equilibrium isotropization in supersymmetric Yang-Mills plasma*, *Phys.Rev.Lett.* **102** (2009) 211601, [[arXiv:0812.2053](#)].
- [39] S. Lin and E. Shuryak, *Grazing Collisions of Gravitational Shock Waves and Entropy Production in Heavy Ion Collision*, *Phys.Rev.* **D79** (2009) 124015, [[arXiv:0902.1508](#)].
- [40] S. S. Gubser, S. S. Pufu, and A. Yarom, *Off-center collisions in AdS(5) with applications to multiplicity estimates in heavy-ion collisions*, *JHEP* **0911** (2009) 050, [[arXiv:0902.4062](#)].
- [41] P. M. Chesler and L. G. Yaffe, *Boost invariant flow, black hole formation, and far-from-equilibrium dynamics in N = 4 supersymmetric Yang-Mills theory*, *Phys.Rev.* **D82** (2010) 026006, [[arXiv:0906.4426](#)].

- [42] P. M. Chesler and L. G. Yaffe, *Holography and colliding gravitational shock waves in asymptotically AdS₅ spacetime*, *Phys.Rev.Lett.* **106** (2011) 021601, [[arXiv:1011.3562](#)].
- [43] O. Aharony, S. S. Gubser, J. M. Maldacena, H. Ooguri, and Y. Oz, *Large N field theories, string theory and gravity*, *Phys.Rept.* **323** (2000) 183–386, [[hep-th/9905111](#)].
- [44] M. P. Heller, R. A. Janik, and R. Peschanski, *Hydrodynamic Flow of the Quark-Gluon Plasma and Gauge/Gravity Correspondence*, *Acta Phys.Polon.* **B39** (2008) 3183–3204, [[arXiv:0811.3113](#)].
- [45] G. Beuf, M. P. Heller, R. A. Janik, and R. Peschanski, *Boost-invariant early time dynamics from AdS/CFT*, *JHEP* **0910** (2009) 043, [[arXiv:0906.4423](#)].
- [46] P. Romatschke and M. Strickland, *Collective modes of an anisotropic quark gluon plasma*, *Phys.Rev.* **D68** (2003) 036004, [[hep-ph/0304092](#)].
- [47] D. T. Son and A. O. Starinets, *Minkowski space correlators in AdS / CFT correspondence: Recipe and applications*, *JHEP* **0209** (2002) 042, [[hep-th/0205051](#)].
- [48] K. Skenderis and B. C. van Rees, *Real-time gauge/gravity duality*, *Phys.Rev.Lett.* **101** (2008) 081601, [[arXiv:0805.0150](#)].
- [49] K. Skenderis and B. C. van Rees, *Real-time gauge/gravity duality: Prescription, Renormalization and Examples*, *JHEP* **0905** (2009) 085, [[arXiv:0812.2909](#)].
- [50] S. Caron-Huot, P. M. Chesler, and D. Teaney, *Fluctuation, dissipation, and thermalization in non-equilibrium AdS₅ black hole geometries*, [arXiv:1102.1073](#).
- [51] D. Mateos and D. Trancanelli, *The anisotropic N=4 super Yang-Mills plasma and its instabilities*, [arXiv:1105.3472](#).
- [52] D. Mateos and D. Trancanelli, *Thermodynamics and Instabilities of a Strongly Coupled Anisotropic Plasma*, [arXiv:1106.1637](#).
- [53] T. Azeyanagi, W. Li, and T. Takayanagi, *On String Theory Duals of Lifshitz-like Fixed Points*, *JHEP* **0906** (2009) 084, [[arXiv:0905.0688](#)].